Catalysis Letters Vol. 108, Nos. 1–2, April 2006 (© 2006)
DOI: 10.1007/s10562-006-0016-z

Comparative analytical study of two Pt–Rh three-way catalysts

J. Hangas* and A.E. Chen
Ford Motor Co., MD3182, 2053, Dearborn, 48121 MI, USA

Received 30 November 2005; accepted 16 January 2006

Pt–Rh three-way catalysts (TWCs) of two formulations were examined by electron probe microanalysis (EPMA) and cross sectional transmission electron microscopy (TEM), in order to study the effect of accelerated aging on microstructure. Both formulations have Pt and Rh applied in separate washcoat layers, Rh in a zirconia-rich outer layer and Pt in an alumina-rich inner layer(s). Microstructural analyses show that in spite of the initial separation, the precious metals inter-diffuse between the washcoat layers and alloy during aging. Following dynamometer aging the two formulations exhibited significant differences in the precious metal (PM) particle size distributions and the correlation between PM particle size and composition. These differences are attributed to the increased transport of Pt due to the presence of ceria and zirconia in the alumina-rich inner washcoat of one formulation, compared to other formulation. The presence or absence of porosity $> 1\mu$m in diameter and differences in initial Pt distributions in the inner washcoat were also noted as possibly contributing to the PM particle growth. The transition alumina of one formulation, containing Ba, partially transformed to corundum during aging. The other formulation utilized a La-stabilized alumina which did not transform to corundum after aging.

KEY WORDS: TEM; EPMA; three-way catalyst; Pt; Rh; diffusion; transport.

1. Introduction

Catalyst technology for automotive emissions control has evolved significantly since the introduction of catalytic converters more than a quarter century ago, but the precious metals, Pt, Pd, and Rh, have always been key ingredients [1, 2]. Pt and Pd, for example, were essential to early oxidation catalysts, later supplanted by Pt–Rh TWCs, which remained the standard for many years. Pd became a suitable replacement for Pt as residual levels of lead in fuel fell, and complex Pd-only formulations were introduced. Meanwhile, due to rising demand throughout the 1990s, Pd became relatively expensive, and the need arose to develop new Pt–Rh TWCs, having performance comparable to the existing Pd and Pd-Rh technology. This paper presents selected results of a comprehensive analytical study of two such Pt–Rh TWCs currently in use. The two formulations were examined in fresh and accelerated aged states to determine the effect of aging on microstructure.

Transition aluminas are widely used as a washcoat support for a portion of the precious metals due to its high surface area. To maintain the surface area during thermal aging, the nanocrystalline transition alumina phase is stabilized to prevent the formation of single crystal corundum (α-Al_2O_3). Ba and Pr have been shown to increase the temperature of the θ-Al_2O_3 to α-Al_2O_3 transformation temperature from 1180 to $\sim$1315 °C, and La increased it to $\sim$1225 °C [3,4]. Individual La atoms have been observed decorating the surface of La stabilizedγ-Al_2O_3 [5]. One formulation examined in this study includes La as a stabilizer for alumina; while the second formulation uses Ba at a similar concentration.

Additional materials added to the washcoat have been shown to affect the PM particle size during high temperature aging. The average PM particle sizes for Pt-only and Pt–Rh catalysts were found to be larger in support materials containing CeO_2 and Al_2O_3 compared to Al_2O_3 alone [6]. Ceria has been reported to promote PM particle growth in the presence of water vapor [7]. Deactivation of Rh deposited on γ-Al_2O_3 by the formation of Rh-aluminates, and the benefits of dispersing Rh on zirconia have been known for some time [8–10].

Previous microstructural studies of TWCs have also documented Pt–Rh alloying and the tendency for the PM particles richest in Rh to be smaller in size. In one model TWC study, powders of Pt/Al_2O_3 and Rh/Al_2O_3 were combined and aged under different atmospheres. Alloying was noted when aged in hydrogen with beneficial effects of increasing light-off performance for HC, NO, and CO conversion. The PM particles with $>$ 15wt% Rh were $<$ 5 nm while the PM particles with $>$ 85wt% Pt ranged from 3 to 15 nm. Pt and Rh remained segregated after aging in air followed by hydrogen aging [9]. Alloying of Pt and Rh and a similar tendency of the resultant PM particle size to be dependent on composition has also been observed in a fully formulated dynamometer-aged single layer TWC where the Pt and Rh were both impregnated after the washcoat support of

* To whom correspondence should be addressed.

alumina and ceria was deposited [11]. The existence of $Ni_xAl_2O_{3+x}$ nanotubes anchoring PM particles was previously reported in dynamometer-aged Pd based and Pt–Rh based TWCs and in vehicle-aged Pd-based TWCs driven 100,000 miles [12, 13].

Although most commercial automotive TWCs segregate Pt and Rh into separate layers, no microstructural study has been done to document particle size distributions and compositions across the washcoats. The present study extends the understanding of the previously mentioned phenomena through electron microscopy methods that retain spatial information of actual washcoat structure and geometry. A comparison will be made of two Pt–Rh catalyst formulations where the Pt and Rh were applied to different washcoat layers, how they both show PM particle alloying, and explain how one formulation has different particle size distributions and compositions than the other formulation.

2. Experimental details

2.1. Samples

The two TWC formulations examined in this study, hereafter referred to as Formulation A and Formulation B, both have a precious metal weight ratio of 5:1 Pt:Rh with a nominal loading of 40 gm/ft^3. Both formulations use multi-channel ceramic monolithic substrates composed of the mineral cordierite with square channels through which the exhaust gas flows. The monoliths had been coated with multiple thin washcoat layers on the cordierite. Monoliths of both catalyst formulations were simultaneously dynamometer-aged using a dual exhaust system for 120 h at a maximum temperature of $\sim$ 1050 °C, and the monoliths were exchanged from side to side midway through the aging cycle. This four-mode dynamometer aging treatment is an accelerated aging test at an elevated temperature intended to simulate 100,000 miles of driving in a short amount of time. Thermocouples were used to monitor the temperatures at the inlet and middle of each monolith during testing and no detectable difference in temperature was observed for the duration of the test. TEM and EPMA samples all came from the middle region of the monolith where temperatures are the highest. A core was taken from this monolith, which was 15cm long. The TEM samples were made from $\sim$ 5–6.4 cm from the inlet, the EPMA sample $\sim$ 6.4–7.5 cm from the inlet.

2.2. EPMA

The EPMA sample core sections were mounted in epoxy, ground and polished, with 1 μm diamond paste providing the final polish. The polished samples were carbon coated to provide a conductive surface layer. The samples were examined in a JEOL 8200 electron microprobe to determine the elemental distributions. An accelerating voltage of 20 keV and a current of 40 nA were used. Wavelength dispersive X-ray (WDX) maps were collected at a resolution of 256$\times$ 256 pixels using beam scanning at 500$\times$ magnification with a 20 ms dwell time. To acquire an adequate signal for the precious metal distributions, background-corrected line scans 1 (μm beam step size) for Pt and Rh were also collected with a 10 s peak and 5 s background collection time.

2.3. TEM

The TEM samples were prepared by vacuum impregnating small pieces of cores with Gatan G-1 epoxy, slicing $\sim$ 0.9 mm thick sections using a low speed diamond saw, and tripod polishing [14]. The wedge angle used in polishing the second side was 3°. Alumina-embedded plastic films were utilized where the smallest grit size was 0.5 μm. The cross-sections were epoxied onto a beryllium support ring and ion milled in a Gatan Precision Ion Polishing System at 3 keV utilizing a graphite stage. The samples were examined either in a JEOL 2000FX TEM equipped with an Oxford energy dispersive X-ray (EDX) analyzer or a JEOL 2010F microscope at the University of Michigan, equipped with a High Angle Annular Dark Field (HAADF) detector and an EDAX EDX analyzer.

To quantify the Pt/Rh composition of each PM particle examined, a Pt/10wt%Rh alloy was used as an analytical standard for EDX spectra. The X-ray lines used for quantitative analysis were the Rh *K* lines at 20.2–20.7 keV (used to avoid the overlap of Rh *L* and Cl *K* lines) and Pt *L*. Desktop Spectrum Analyzer (DTSA) version 2.5 by NIST was used to quantify the spectra from the EDAX analyzer, and Oxford software was used to quantify spectra from the Oxford analyzer. The Pt–Rh quantitative results reported here are estimated to be accurate to within 5% relative based on "thin film criterion" calculations for a PM particle embedded at the bottom of a foil consisting either of ceria or alumina.

3. Results

3.1. Formulation A

EPMA element distribution maps of fresh and dynamometer-aged Formulation A are shown in figure 1. The inner washcoat is primarily Ba-stabilized transition alumina with zirconia–ceria and ceria added as separate phases. The outer washcoat is primarily zirconia–ceria with Ba-stabilized alumina agglomerates. Nickel in the inner layer was added in the form of NiO in micron-sized particles as identified by TEM. The NiO disperses and interdiffuses with the alumina upon dynamometer aging and Ni is found in three forms in TEM: (1) clusters of small solid $Ni_xAl_2O_{3+x}$ spinel grains $< 0.2\mu$m with $x \leq 0.4$ reside in pores near the original location of the NiO agglomerate, (2) minor to trace amounts dispersed in the

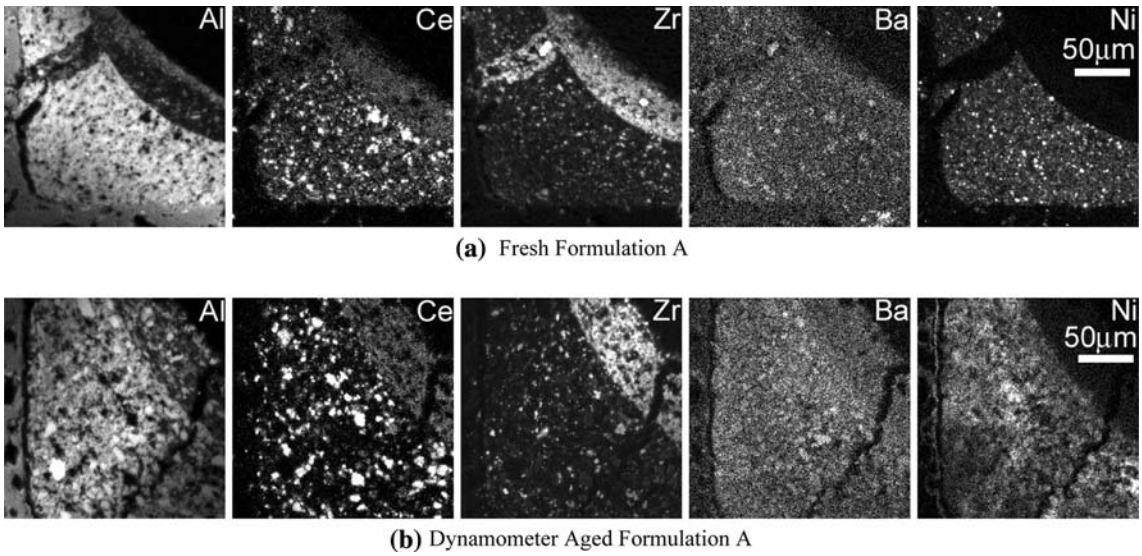

Figure 1. Electron microprobe element distribution maps of Formulation A in the fresh and dynamometer aged condition. The crack observed in the fresh sample is from shrinkage of the inner layer during drying, which is then filled by the outer layer when it is applied. This is often seen in fully formulated catalysts.

alumina agglomerates and trace amounts in ceria agglomerates, and (3) $Ni_xAl_2O_{3+x}$ nanotubes, the growth of which is assisted by the PM particles. No residual NiO has been identified by TEM or STEM after aging.

Quantitative line scans by EPMA reveal that in fresh Formulation A, Pt is present at 0.5–1.0 wt% throughout the inner washcoat while Rh is present at lower concentrations throughout the outer washcoat (figure 2a). TEM analysis of fresh Formulation A detected 10 nm Pt particles present in the inner washcoat alumina. No Pt particles were observed to be associated with ceria or zirconia–ceria phases. This non-uniformity in the distribution of Pt particles is consistent with the variable signal strength of Pt in the inner washcoat EPMA line scan of figure 2a. Rh particles were too small to be detected by TEM in the outer washcoat of the fresh sample.

Coarsening of Pt due to dynamometer aging was detectable in EPMA by the sharpening of the Pt peaks present in line scans (figure 2b). Examination of line scans for cerium and aluminum (not shown here) identifies the interface between the inner and outer washcoats at 60 μm for this analysis. This corresponds to the location of the highly correlated peaks of Pt and Rh, indicating alloying of these elements. The lines scans show that Rh has diffused into the inner washcoat as far as 50 μm while a smaller (and less obvious due to the low concentration of Pt) amount of Pt has apparently diffused into the outer washcoat.

Detailed measurements of the diameter and composition of individual PM particles as a function of distance from the outside surface of the washcoat was determined by analyzing a TEM cross-section of the dynamometer-aged washcoat. Figure 3a shows a low magnification photographic montage of the inner and

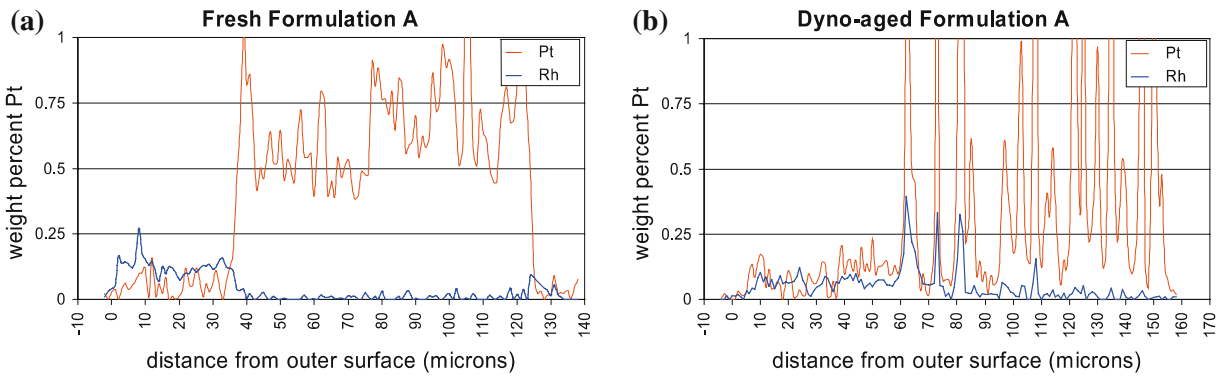

Figure 2. Line scans of precious metals in fresh (a) and dynamometer-aged (b) Formulation A. Evidence of coarsening of the PM particles as well as alloying of the Pt and Rh is seen in the dynamometer-aged sample.

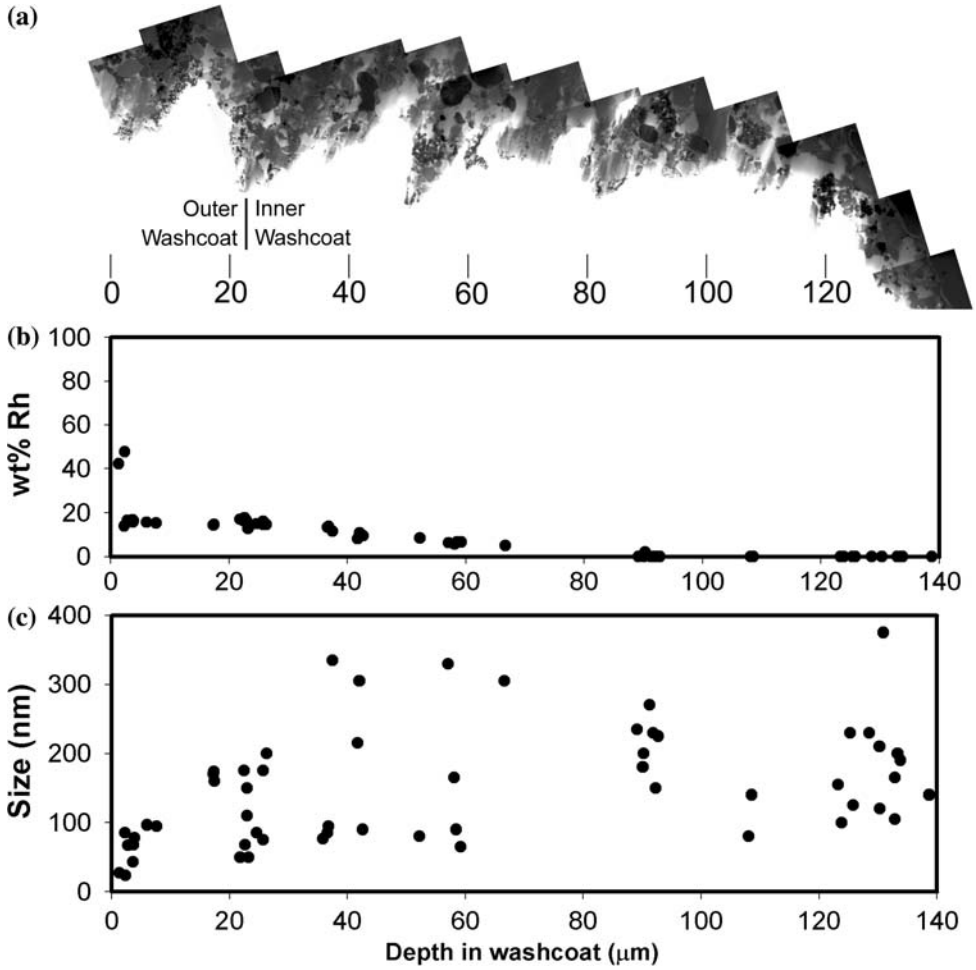

Figure 3. Cross-section of Formulation A. (a) Montage of TEM images through the entire washcoat showing that useable thin area was present throughout the cross section. The outer surface is at left and the cordierite substrate is at the right. (b) Wt% Rh versus depth in washcoat measured from the outer surface and (c) PM particle size vs. depth into the washcoat.

outer washcoats. The interface between the inner and outer washcoats was determined by the abrupt change in the distribution of zirconia at this location. Measurements were made at higher magnification (≥ 100,000×) of the PM particle diameter and composition, and these results are summarized in figure 3b and c. The two smallest PM particles (~25 nm in diameter) were observed at the outer surface of the washcoat and contained approximately 40wt% Rh. There is a large drop in average Rh concentration to ~15wt% Rh a few microns from the outer washcoat surface, and this alloy composition remains constant through the rest of the outer washcoat where the PM particles are observed to be located directly on zirconia–ceria grains. This result is at least in part consistent with the EPMA line scan data which shows a higher level of Pt compared to Rh near (between 40 and 60 μm) the boundary between the two washcoat layers. Despite a large variation in PM particle size at any particular location in the washcoat, figure 3c also shows a general tendency of increasing PM particle size with increasing depth into the outer washcoat with 50–200 nm particles located at the bottom of the outer washcoat (~25μm below the outer washcoat surface). In the inner washcoat there is a gradual decrease in Rh concentration with increasing depth, until at a depth of ~ 90μm the concentration is less than the minimum detectable mass (~2wt% Rh). PM particle size ranges from 40 to 375 nm throughout the inner washcoat, with the smallest PM particles located inside alumina agglomerates, and the larger particles anchored on $Ni_xAl_2O_{3+x}$ nanotubes (figure 4) and located in channels or in pores between the ceramic agglomerates. Such nanotubes do not exist in the outer washcoat due to the lack of Ni. Pores 1 μm wide and a few microns long are frequent throughout both washcoats.

The transition alumina in both the fresh and aged material had a crystallite size of 5 nm wide and 20 nm long. Selected area diffraction (SAD) patterns of the fresh and aged transition aluminas were identical. Each had only a few diffuse rings. The two strongest rings with *d*-spacings of 0.20 and 0.14 nm are consistent with strong reflections in several γ-Al_2O_3 powder diffraction

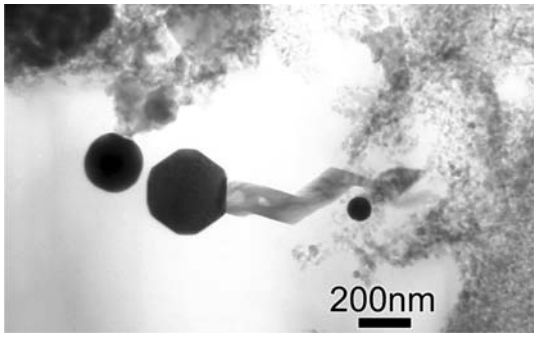

Figure 4. Nanotube of $Ni_xAl_2O_{3+x}$, below center, anchors a Pt/Rh particle and suspends that particle in a pore. The nanotube has been tilted close to a zone axis and bend contours are visible. The other two Pt–Rh particles are anchored on shorter aluminate deposits.

patterns and one δ-Al_2O_3 pattern. Reflections with d-spacing > 0.24 nm such as 111_γ are missing. Although no corundum was found by TEM or XRD in the fresh material, corundum was observed to coexist with the transition alumina in aged Formulation A. The corundum crystals were observed in TEM to be equiaxed and sub-micron in size, and contained only trace levels of Si (detected by EDX). A few corundum crystals were found in the outer washcoat. The distribution of corundum in the inner washcoat was highly variable with some agglomerates of transition alumina observed to contain no corundum crystals while others contained many corundum crystals (figure 5). The frequency of corundum grains could not be correlated with the distribution of either Ba (which in the untransformed alumina was within the range found in the fresh material of 2.5–3.5wt%), Ni (which ranges from 3 to 12wt% in the untransformed alumina), or the distribution of PM particles. A few corundum crystals were also identified in the outer washcoat region.

3.2. Formulation B

The inner washcoat of Formulation B is La-stabilized alumina. Minor amounts of ceria–zirconia are also present in scattered agglomerates. WDX maps (figure 6a) of the fresh inner washcoat show it is applied in several layers with no apparent difference in composition between the layers, although the bottom layer has higher porosity. NiO is added as small agglomerates which vary in local distribution. Maps of other locations show a more uniform distribution pattern of NiO between the layers of the inner washcoat. The outer washcoat is primarily ceria–zirconia with some La-stabilized transition alumina agglomerates a few microns in diameter (figure 6a).

The bulk distribution of elements following dynamometer aging shows little change from the fresh sample except for the distribution of Ni (figure 6b). Dynamometer aging of this formulation produces a very non-uniform distribution of Ni compared to Formulation A,

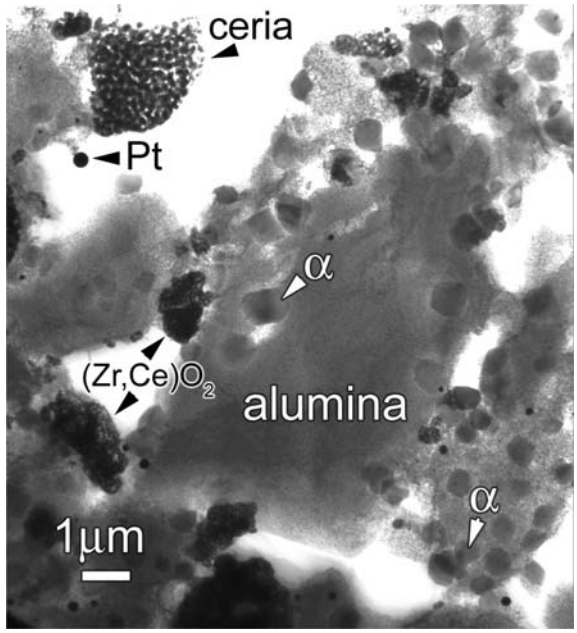

Figure 5. TEM image of general microstructure of aged Formulation A at a depth of 70 μm in figure 3, showing ceria agglomerates (dark with fine internal porosity), fine-grained aggregates of zirconia–ceria, transition alumina (mottled grey), Pt–Rh particles, and crystals of corundum (α-Al_2O_3) that occur in varying densities in different alumina agglomerates.

with several large regions 10–15 μm in diameter exhibiting very high Ni concentration.

EPMA line scans of fresh Formulation B showed that Rh was present throughout the outer washcoat. Pt concentration was highest at the top of the inner washcoat and decreased rapidly with increasing depth but was still detectable throughout the inner washcoat (figure 7a). Pt is below minimum detectable mass in the outer washcoat, such that the line scan shown for figure 7a only shows noise for the Pt signal in the outer washcoat. Following dynamometer aging the Pt signal from Formulation B becomes much more 'spiky', similar to formulation A, indicating coarsening of the Pt particles (figure 7b). Although the migration of Pt and Rh across the interface separating the outer and inner washcoats is noticeable (Rh migrates into the inner layer as much as 15 microns and Pt to within 30 μm of the outside edge) the correlation of strong Pt and Rh signals observed for Formulation A does not exist because the PM particle size is smaller.

TEM measurements of composition and size of individual PM particles for dynamometer-aged Formulation B (figure 8) show a general trend of decreasing Rh content and increasing PM particle size with depth. The Rh concentrations of PM particles found at the outer surface were again the highest in the sample: 91% and 99.6%Rh, and the latter was the smallest PM particle detected at 11 nm in diameter. The composition rapidly drops to $\sim$ 50wt% Rh a few microns from the outer surface but then rises to $\sim$ 60wt% Rh between the depths of 10–15 μm and

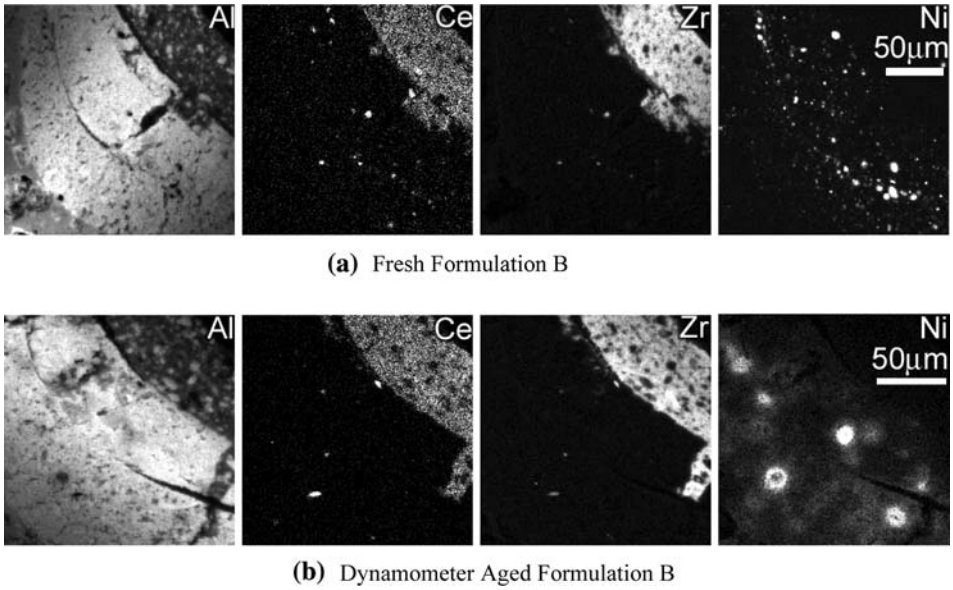

Figure 6. Electron microprobe element distribution maps of Formulation B.

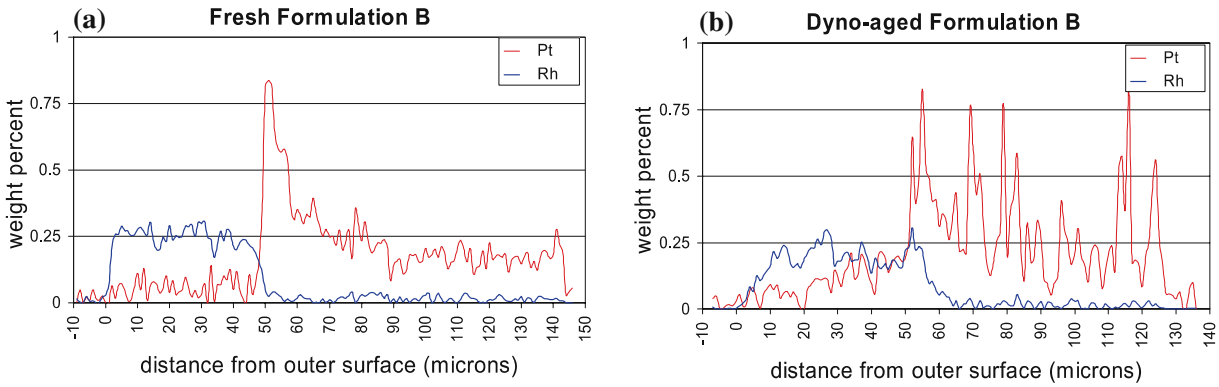

Figure 7. Line scans of precious metals in fresh (a) and dynamometer-aged (b) Formulation B. In the fresh catalyst, there is a distinction between the inner (Pt) and outer (Rh) layers. This distinction is not seen in the dynamometer-aged catalyst, due to migration of the Pt and Rh. The sharp peaks in the plots of the dynamometer-aged catalyst indicate a coarsening of the Pt particles.

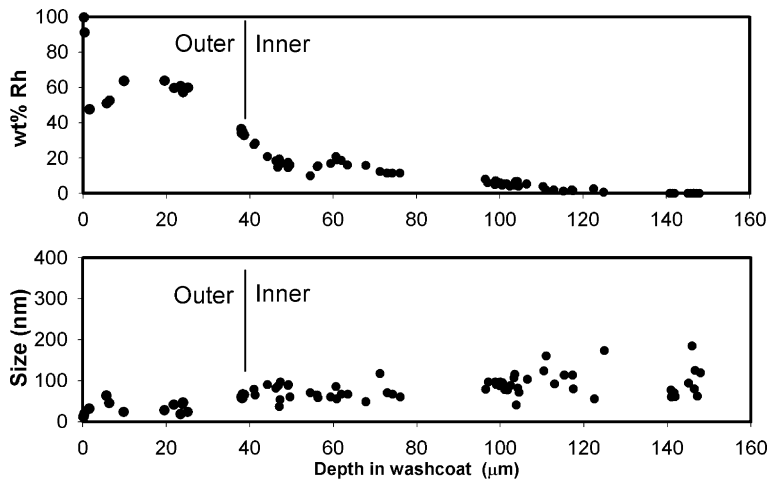

Figure 8. The PM particle composition and size vs. depth in the washcoat for Formulation B. The boundary between the inner and outer washcoat is at 40 μm.

then declines gradually until no Rh is detectable at a depth of about 140 μm. The small inflection upward in Rh concentration at a depth of 60 μm is presumably due to the proximity of a shrinkage crack in the inner washcoat which had become filled with outer washcoat material. Similar to Formulation A, PM particles in the outer washcoat rest directly on the zirconia–ceria grains, and larger PM particles in the inner washcoat were mainly on $Ni_xAl_2O_{3+x}$ nanotubes which had grown into pores between alumina agglomerates. TEM detected concentration variations of 1–6wt% Ni in alumina agglomerates in different regions of the inner washcoat of the cross section. Small solid 35 nm grains of $Ni_xAl_2O_{3+x}$ with 18wt% Ni ($x \approx 0.4$) were found in pores next to the alumina with 6wt% Ni, and these were probably the locations of NiO agglomerates in the starting material. These results are consistent with the inhomogeneous distribution of Ni detected in EPMA X-ray map. No significant correlation was observed between PM particle size and the Ni content of the transition alumina.

The outer washcoat is densely packed, and the largest pores are submicron. In the TEM cross section of the aged sample, the inner washcoat had two layers with different porosity. The top layer of these extended to a depth of 76 μm. The alumina agglomerates in it were well packed, and porosity or passages around them was submicron in width. The average PM particle in this layer was 71 ± 18 nm. The bottom layer had significant porosity with dimensions of 1–4 μm and a PM particle size of 103 ± 53 nm, and Rh content of the PM particles is < 5wt%. A gap in the data between the depths of 76 and 96 μm is due to a crack between the two inner layers.

The alumina in Formulation B was stabilized with approximately 3wt% La, and no corundum was found in the aged catalyst. Trace amounts of Si were also detected in the fresh material, but Si increased to up to 3wt% in the alumina of the aged material near the cordierite. The SAD pattern from the alumina had only a few diffuse rings. The strongest was at 0.24 nm, followed by 0.20 and 0.14 nm. As in Formulation A, these rings are common to γ-Al_2O_3 and δ-Al_2O_3, and d-spacings larger than 0.24 nm are missing, such as 111_γ.

4. Discussion

The results of this study show that Pt and Rh applied in separate washcoat layers are transported across the washcoat boundary and alloy during sufficiently harsh (thermal) aging. EPMA line scans for aged Formulation A detected a relatively constant trace level of Pt lower than the Rh concentration in the outer washcoat (figure 2), while TEM detects 18wt% Rh in the particles there (figure 3). This suggests that there may be some Rh present dispersed in smaller particles that TEM did not have the analytical sensitivity to detect. The EPMA and TEM results are consistent in the outer washcoat of Formulation B where both detect a steeper concentration gradient (figure 8).

The two formulations show significantly different behavior in a plot of PM particle size vs. wt% Rh (figure 9). Formulation A shows no correlation between particle size and composition with virtually all particles containing $\leq$ 18wt% Rh and distributed parallel to the particle size axis of figure 9. Particles $< 125\mu$m in

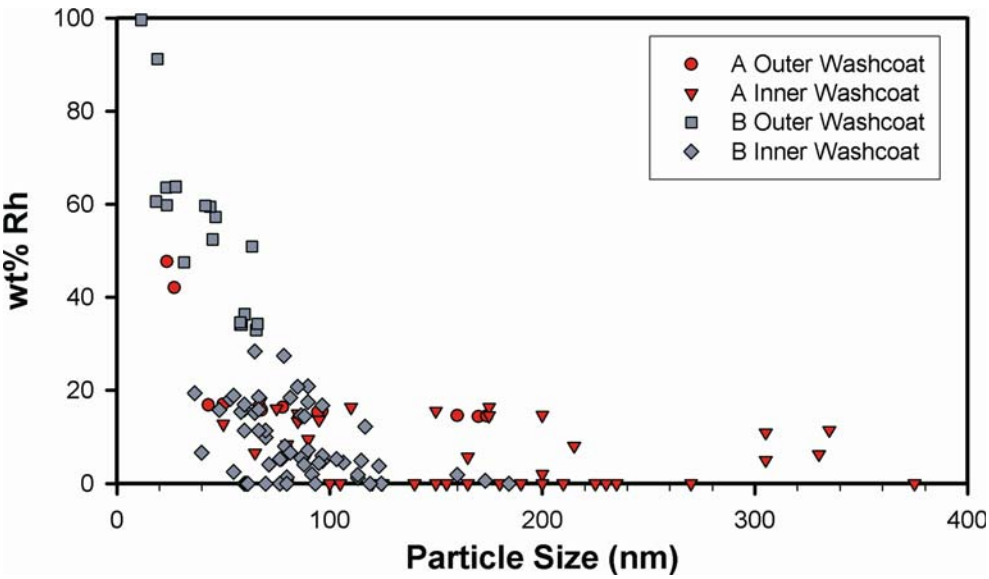

Figure 9. The plot of Pt–Rh particle size vs. wt% Rh in both aged samples shows two regimes. One where there appears to be an envelope of correlation between PM particle size and composition more pronounced in Formulation B, and the other where there is none as in most of Formulation A.

diameter show an inverse correlation between wt% Rh and particle diameter in the outer washcoat.

A high Rh content has been reported to reduce PM particle growth, presumably due to the lower vapor pressure of Rh_2O_3 than PtO_2 [6, 9, 15]. These two catalyst formulations had identical amounts of Pt and Rh initially separated in different washcoat layers but have drastically different particle size and composition distributions following identical aging treatments. Clearly other phenomena must affect the coarsening of the PM particles in addition to Pt and Rh alloying.

The main difference between formulations that could cause the higher mobility of Pt for PM particle growth is that ceria (which is known to promote PM particle growth [6]) and zirconia are present in the inner washcoat of Formulation A vs. their absence in B. Other contributing factors that may promote the difference in particle growth between samples are: (1) Formulation A has more porosity $>1\mu$m in diameter (porosity $>1\mu$m in width does not occur in Formulation B until a depth of $>110\mu$m) and (2) the initial Pt distribution in the inner washcoats (concentrated near the top of the inner washcoat in B). Particle size in Formulation B may be slightly moderated by the distribution of Pt close to the top of the inner washcoat, while Formulation A should have more uniform particle growth across the washcoat.

No segregation of Pt or Rh within individual PM particles was detected in a FEG TEM where the smallest useful beam size for EDX analysis was 5 nm. The cycling of air/fuel ratio around stoichiometric combustion conditions produced exhaust gas conditions sufficiently inert that full alloying of the PM particles was possible [16]. In both aged formulations the particles with the highest Rh content were on the outer exhaust gas surfaces (depth ≈ 0) and were $>$ 20 wt% higher in Rh than particles a few microns from the surface. The higher Rh content of these PM particles, and conversely the lower Pt content, suggests that some environmental variable at the surface such as the gas flow reduces the ability of Pt to alloy with Rh at the surface.

The largest PM particles found in this study were on $Ni_xAl_2O_{3+x}$ nanotubes located in pores. The location in pores would be the most suitable for growth by vapor phase, since the PM particles in pores would receive the highest gas flow. No work has been done to determine how early nanotubes nucleate and grow.

Formation of α-Al_2O_3 is undesirable for maintaining high surface area in the washcoat. The α-Al_2O_3 observed in Formulation A is equiaxed, indicating that its growth was not assisted by PM catalyst particles that would have produced a whisker morphology. No phases were observed to be trapped inside α-Al_2O_3 grains, unlike what was observed by More *et al.* [11]. This observation suggests slower α-Al_2O_3 crystal growth occurred in this study. The reasons for the failure of Ba to completely stabilize the transition alumina in Formulation A are not clear. SAD analysis failed to identify which γ, δ, θ, or some other transition alumina is present. It is possible that there is a small amount of an easily transformable transition alumina present in Formulation A. About 3wt% of Ba and La were found in the alumina of Formulations A and B, respectively, as determined by EDX analysis. This concentration of La is more than the minimum amount needed to stabilize the alumina, but substantially less than the amount where $LaAlO_3$ has been observed to form [4]. No correlation was seen between the current distribution of elements present in aged Formulation A, such as Ni, Si, and PM particles, and the distribution of α-Al_2O_3.

5. Conclusions

Formulations A and B are both production automotive Pt–Rh TWCs that have Rh applied in a zirconia–ceria outer washcoat layer and Pt applied in an alumina-rich inner washcoat layer(s). Formulation B has less ceria and zirconia added to the inner alumina washcoat layers, compared to Formulation A. In spite of the attempt to segregate the Pt and Rh in separate layers, the precious metals are transported between layers during dynamometer aging, as observed in both EPMA and TEM. In TEM cross sections of the dynamometer aged materials, PM particles on the surface of the outer washcoats are richest in Rh and gradually tapers to zero at depths of 80–120μm into the washcoat. Formulation B showed some correlation between increasing PM particle size and decreasing Rh content. Formulation A showed no correlation between PM particle size and composition, and the average PM particle size was twice that found in Formulation B. The difference in PM particle size vs. composition is consistent with the promotion of PM particle growth by the presence of ceria and zirconia–ceria agglomerates in the alumina of the inner washcoat. PM particle growth is assisted by the more open porosity throughout Formulation A. In comparison, Formulation B was more densely packed and had few ceria particles in the alumina-rich inner washcoat.

Acknowledgments

We would like to thank Art Kolasa for providing the dynamometer-aged samples, and Kelly Weigand, Mark Jagner, and Charlotte Lowe-Ma for providing XRF and XRD results (not presented). We wish to thank George Graham, Bill Donlon, and Bob McCabe for many useful discussions and critical reading of this paper. The JEOL 2010F at the Electron Microbeam Analysis Laboratory at the University of Michigan was purchased under NSF grant DMR-9871177.

References

[1] H.S. Gandhi, G.W. Graham and R.W. McCabe, J. Catal. 216 (2003) 433–442.

[2] M. Shelef and R.W. McCabe, Catal. Today 62 (2000) 35–50.
[3] S. Rossignol and C. Kappenstein, Int. J. Inorg. Mater. 3 (2001) 51–58.
[4] T. Yamamoto, T. Hatsui, T. Matsuyama, T. Tanaka and T. Funabiki, Chem. Mater. 15 (2003) 4830–4840.
[5] S. Wang, A.Y. Borisevich, S.N. Rashkeev, M.V. Glazoff, K. Sohlberg, S.J. Pennycook and S.T. Pantelides, Nat. Mater. 3 (2004) 143–146.
[6] R. Polvinen, M. Vippola, M. Valden, T. Lepistö, A. Suopanki and M. Härkönen, J. Catal. 226 (2004) 372–381.
[7] J. Barbier Jr. and D. Duprez, Appl. Catal. B 4 (1994) 105–140.
[8] H.C. Yao, S. Japar and M. Shelef, J. Catal. 50 (1977) 407–418.
[9] Z. Hu, F.M. Allen, C.Z. Wan, R.M. Heck, J.J. Steger, R.E. Lakis and C.E. Lyman, J. Catal. 174 (1998) 13–21.
[10] H.C. Yao, H.K. Stepien and H.S. Gandhi, J. Catal. 61 (1980) 547–550.
[11] Karen L. More, E.A. Kenik, D.W. Coffey, T.S. Geer, W.J. Labarge, R. Beckmeyer and J. Theis, SAE Paper No. 972905, in: *Topics in General and Advanced Emission*, (SAE Special Publication SP-1296, 1997) 183–191.
[12] J. Hangas, Catal. Lett. 86 (2003) 267–272.
[13] J. Hangas, Microscopy and Microanalysis 10(Suppl. 2) (2004) 440–441.
[14] J. Benedict, Ron Anderson, S. J. Klepeis and M. Chaker, in: S*pecimen Preparation for Transmission Electron Microscopy of Marterials-II*, ed. R. Anderson, Mater. Res. Soc. Proc. 199, (Pittsburgh, PA USA, 1990) p. 189.
[15] H.C. Yao, M. Sieg and H.K. Plummer, J. Catal. 59 (1979) 365.
[16] M. Chen, T. Wang and L.D. Schmidt, J. Catal. 60 (1979) 356.